RSC Advances

PAPER

View Article Online
View Journal | View Issue

Cite this: *RSC Adv.*, 2021, **11**, 35585

Application potential of biogenically synthesized silver nanoparticles using *Lythrum salicaria* L. extracts as pharmaceuticals and catalysts for organic pollutant degradation†

Nikola Z. Srećković,[a] Zoran P. Nedić,[b] Davide Liberti,[c] Daria Maria Monti,[c] Nevena R. Mihailović,[a] Jelena S. Katanić Stanković,[d] Silvana Dimitrijević[e] and Vladimir B. Mihailović *[a]

This study was designed to evaluate the optimal conditions for the eco-friendly synthesis of silver nanoparticles (AgNPs) using *Lythrum salicaria* L. (Lythraceae) aqueous extracts and their potential application and safe use. AgNPs synthesized using *L. salicaria* aerial parts (LSA-AgNPs) and root extract (LSR-AgNPs) were characterized by UV-Vis spectrophotometry, Fourier transform infrared spectroscopy (FTIR), scanning electron microscopy (SEM/EDS), and X-ray powder diffraction (XRPD). Dynamic light scattering (DLS) was used for the determination of the size distribution profiles of the obtained nanoparticles. Both *L. salicaria* extracts showed high phenolic content, while the flavone *C*-glucosides orientin, vitexin, and isovitexin were detected in extracts using HPLC. The synthesized AgNPs displayed growth inhibition of the tested bacteria and fungi in concentrations between 0.156 and 1.25 mg mL^{-1}. The studied nanoparticles also showed antioxidant potential and gained selectivity at different concentrations on different cancer cell lines. Concentrations of LSA-AgNPs were found to be 20.5 and 12 μg mL^{-1} towards A431 and SVT2, respectively, while LSR-AgNPs were effective only against A431 cancer cells (62 μg mL^{-1}). The hemolytic activity of LSA-AgNPs in concentrations up to 150 μg mL^{-1} was not observed, while LSR-AgNPs in the highest applied concentration hemolyzed 2.8% of erythrocytes. The degradation possibility of Congo red and 4-nitrophenol using LSA-AgNPs and LSR-AgNPs as catalysts was also proven. The results indicate that *L. salicaria* may be used for the eco-friendly synthesis of AgNPs with possible applications as antimicrobial and selective cytotoxic agents towards cancer cell lines, as well as in catalytic degradation of pollutants.

Received 20th July 2021
Accepted 22nd October 2021

DOI: 10.1039/d1ra05570d

rsc.li/rsc-advances

1. Introduction

Nanoparticle's research is a topic of dynamic scientific exploration nowadays, emphasizing nanoparticle application in various fields such as electronics, catalysis, biosensors, wastewater treatment, biomedicine, pharmaceuticals, and cosmetics.[1] Due to the rising industrial uses of nanoparticles, their production volume is constantly increasing, and their synthesis is mainly based on physical and chemical methods that consume a lot of energy or need the use of potentially environmentally harmful chemical compounds.[2] Nanobiotechnology aims to establish low-cost and environmentally suitable methods for use of some biological components or live organisms and their products for the fabrication of different nanoparticles. It has been reported that bacteria, fungi, molds, and plants may be used for the successful synthesis of nanoparticles in an environmentally acceptable manner.[3,4] However, the use of some natural resources such as microorganisms in nanoparticle synthesis risks possible negative effects on health and environmental contamination. Some plant extracts or phytochemicals, particularly obtained from medicinal herbs and spices, have greater potential in nanoparticle synthesis compared with microorganisms. In addition to provide environmentally friendly reducing and stabilizing agents for the formation of the nanoparticles, these plant-originated products may possess beneficial biological characteristics and transfer their properties to nanoparticles during synthesis.[5] Plant

[a]*University of Kragujevac, Faculty of Science, Department of Chemistry, Radoja Domanovića 12, 34000 Kragujevac, Serbia. E-mail: vladimir.mihailovic@pmf.kg.ac.rs*
[b]*University of Belgrade, Faculty of Physical Chemistry, Studentski trg 12-16, P.O. Box 47, 11159 Belgrade, Serbia*
[c]*University of Naples Federico II, Complesso Universitario Monte Sant'Angelo, Department of Chemical Sciences, via Cinthia 4, 80126, Naples, Italy*
[d]*University of Kragujevac, Institute for Information Technologies Kragujevac, Department of Science, Jovana Cvijića bb, 34000 Kragujevac, Serbia*
[e]*Mining and Metallurgy Institute Bor, Zeleni bulevar 35, 19210 Bor, Serbia*

† Electronic supplementary information (ESI) available. See DOI: 10.1039/d1ra05570d

phenolic compounds are well-known secondary metabolites with valuable pharmacological properties and their emphasized redox characteristics. Their redox capacity provides them an opportunity to be used as reducing agents of metal ions during plant-mediated synthesis of metal nanoparticles, while their structure is responsible for stabilizing obtained nanoparticles.[6]

Among different metal-based nanoparticles that are in use, silver nanoparticles (AgNPs) have a long history of application primarily because they possess antimicrobial properties.[7] AgNPs are used in cosmetic preparations, as a catalyst in the chemical industry, for biomedical purposes, and preparation of material with antimicrobial properties.[8] The use of AgNPs for medicinal or food packaging purposes is in increase and their synthesis using plant extracts could be a great advantage considering the ecological aspect of the synthesis process and supplementing of nanoparticles themselves with biologically important compounds.[9,10]

Different nanoparticles, including AgNPs, have been reported as effective catalysts in the degradation of harmful diazo dyes from various industries.[11] Oxidation or photolysis is not a common pathway of degradation of stable azo dyes and they can remain unchanged for years.[12] Therefore, the treatment of wastewater containing such dyes is essential for the preservation of the environment.[13]

Lythrum salicaria L. (Lythraceae) is native in Europe and Asia, as well as in some areas in Africa and Australia. In North America, *L. salicaria* (purple loosestrife) has been introduced and now it is on the red list because of its strong invasive ability. Purple loosestrife is also known for its traditional use in the treatments of inflammatory disorders (dysentery, hemorrhoids, intestinal catarrh, and eczema).[14] Previously published results showed that *L. salicaria* possesses high polyphenolic content and excellent antioxidant properties. Its root is particularly rich in tannins, while the aerial part contains characteristic *C*-glycosides vitexin, orientin, isovitexin, and isoorientin.[14,15] *L. salicaria* aerial part extract was used in a previous study conducted by Mohammadalinejhad *et al.* for synthesis of AgNPs for the fabrication of nanohybrids with cellulose, chitosan, and lignocellulose.[16] However, the root extract of *L. salicaria* which possesses high antioxidant potential[15] has not been studied for nanoparticle synthesis, as well as detailed biological properties of *L. salicaria* fabricated nanoparticles have not been examined so far. The main goal of this study is to determine and optimize the conditions for the ecologically friendly synthesis of AgNPs using aerial part (LSA) and root (LSR) aqueous extracts of *L. salicaria*. Considering the invasiveness of *L. salicaria* and due to the need for reduction of its population in some areas (especially in North America), the focus of this research was the prospective application of *L. salicaria* in the environmentally friendly synthesis of AgNPs and potential applications of obtained nanoparticles as antimicrobial, antioxidant, and cytotoxic agents. Considering catalytic properties of AgNPs, degradation of Congo red day and 4-nitrophenol in presence of obtained nanoparticles was also determined.

2. Methods and materials

2.1. Materials

The chemicals used in this study (sodium borohydride ($NaBH_4$), silver nitrate ($AgNO_3$), 2,2′-azino-bis(3-ethylbenzthiazoline-6-sulfonic acid) (ABTS), sodium dodecyl sulfate (SDS), 2,2-diphenyl-1-picrylhydrazyl 1,1-diphenyl-2-picrylhydrazyl radical (DPPH), referent phenolic standards, and methanol) were procured from Sigma-Aldrich Chemicals (Deisenhofen, Germany). Substrates and components (Nutrient agar (NA), Sabouraud Dextrose Agar (SDA), Müller–Hinton broth (MHB), and Sabouraud Dextrose Broth (SDB)) for microorganisms' cultivation and determination of antimicrobial activity are provided from Torlak Institute of Virology, Vaccines, and Sera (Belgrade, Serbia). The resazurin salt was supplied from Acros Organics (New Jersey, USA). Solvents used in high-performance liquid chromatography (HPLC) analyses were obtained from Roth (Karlsruhe, Germany).

2.2. Preparation of *L. salicaria* extracts

L. salicaria was collected in village Veliko Krčmare (Central Serbia) in August 2017. The plant material was identification at the Herbarium of the Department of Biology and Ecology, Faculty of Science, University of Kragujevac, Serbia (voucher number 130/018). To remove any impurities, the plant material was rinsed with deionized water, dried at room temperature in a dark area, and powdered using a laboratory mill. The powdered dried aerial (LSA) and root (LSR) plant materials (10 g) were separately added to 100 mL of boiling deionized water. After 1 h, the obtained extract was filtered with Macherey-Nagel 85/70 mm filter paper. Aqueous extracts were stored at 4 °C for further use within a week.

2.3. Phytochemical assessment of *L. salicaria* aqueous extracts

Total phenolic and flavonoid contents were estimated spectrophotometrically as described previously.[15] Total phenolic content expressed as milligrams of gallic acid equivalents per gram of dry plant weight (mg GAE per g dry plant) was determined using the Folin–Ciocalteu reagent. The quantification of total flavonoids in extracts expressed in milligrams of quercetin per gram of dry plant weight (mg QUE per g dry plant) was determined using the method with aluminum chloride as reagents for the formation of yellow compounds with flavonoid compounds. All experiments for the determination of total phenolic and flavonoid contents were performed in three replications.

The chromatographic analyses of phenolic compounds in *L. salicaria* aqueous extracts were performed using the HPLC system (Shimadzu Prominence, Kyoto, Japan) configured with a Photodiode Array Detector (SPD-M20A). For separation of phenolic compounds, a Phenomenex Kinetex® (Phenomenex, Torrance, CA, US) C18 column (100 × 4.6 mm, 2.6 μm particle size) thermostated at 40 °C was used. The mobile phase used for the separation of phenolic compounds was Millipore water (phase A) and acetonitrile (phase B) with the addition of trifluoroacetic acid (0.1% in both phases). Gradient mode 0–1 min 5% B, 1–10 min 5–30% B, and 10–15 min 100% B was applied. The solvent flow rate during chromatographic separation was 2 mL min^{-1} after injection of 10 μL of sample extracts.[17] The chromatograms were recorded at wavelengths 280, 325, and 360 nm and analyzed using LC Solution software version 1.24 SP1 (Shimadzu, Kyoto, Japan).

For the identification of compounds in extracts, the retention times and UV-Vis absorption spectra obtained for reference

standards were compared with corresponding data obtained for chromatograms of extracts. The calibration lines for vitexin, isovitexin, and orientin were drawn using different concentrations of corresponding referent standards and used for quantification of these compounds in extracts.

2.4. Biosynthesis of AgNPs

Different reaction conditions were applied for the synthesis of nanoparticles using the aerial part (LSA-AgNPs) and root (LSR-AgNPs) extracts of *L. salicaria*. Silver nitrate was dissolved in diluted (2.5, 5, 10, and 20%, v/v) LSA and LSR aqueous extracts to obtain different concentrations of $AgNO_3$ (0.5, 1, 10, and 20 mM). The reaction mixtures were stirred on a magnetic stirrer and heated at different temperatures (25, 50, and 80 °C) until metal nanoparticles were formed. To modify the pH of the reaction mixture (pH 2, 6, and 12) 1 M HNO_3 or 1 M NaOH were used. Visual color change (from light yellow to dark brown) and UV-Vis spectrophotometry were used to observe the production of AgNPs throughout the synthesis. The best conditions for the highest LSA-AgNPs yield production were: 20 mM concentration of $AgNO_3$, 5% (v/v) aerial part extract concentration, a reaction temperature of 25 °C, pH 12, and reaction time of 30 min for synthesis. The best reaction conditions for the LSR-AgNPs production were as follows: 10 mM $AgNO_3$ concentration, root extract concentration 10% (v/v), a reaction temperature of 80 °C, pH 12, and reaction time 30 min. After the synthesis of AgNPs, the suspensions were centrifuged at 12 000 rpm for 10 min. Obtained residue after centrifugation resuspended in demineralized water, centrifugated again, and the precipitated nanoparticles were then dried in a hot air oven (40 °C) and stored at 4 °C.

2.5. Characterization of synthesized AgNPs

A double beam spectrophotometer Halo DB-20S (Dynamica GmbH, Switzerland) was used to monitor the synthesis of AgNPs in the wavelength range 300–800 nm with a resolution of 0.5 nm. The X-ray diffractometer (PHILIPS PW 1710) set at a voltage of 40 kV and 30 mA with CuKα radiation of 1.54178 Å was used to analyze the crystal structure of the biosynthesized nanoparticles. The samples were tested in the range of 10–90° 2θ with a step of 0.02° and a retention time of 0.25 s at each step. A scanning electron microscope (SEM) JOEL JSM IT 300LV with EDS detector (OXFORD Instruments, X-max) was used to examine the surface and elemental composition of nanoparticles. The samples for SEM were prepared in JOEL FC-TM20 auto coating thickness controller. For the determination of nanoparticles size, dynamic light scattering (DLS) measurements were carried out using Mastersizer 2000 from Malvern Panalytical. Obtained nanoparticles samples, as well as dry extract used in their synthesis, were subjected to Fourier transform infrared spectroscopy (FTIR) for the detection of functional groups of molecules present in samples.

2.6. Antioxidant activity

The antioxidant activity of AgNPs was studied using two $ABTS^{\bullet+}$ and $DPPH^{\bullet}$ scavenging assays.[15] Different concentrations of LSA-AgNPs and LSR-AgNPs aqueous solutions were mixed with ABTS methanol solution. After 30 minutes of incubation at room temperature in the dark, the absorbance was measured at 734 nm. Similarly, serial dilutions of obtained nanoparticles in water were mixed with the same volume of $DPPH^{\bullet}$ solution to test the ability of nanoparticles to neutralize the DPPH radicals. After standing in the dark place for 30 min the absorbance of the solution mixture of DPPH radicals and nanoparticles was measured spectrophotometrically at 517 nm. As a reference antioxidant butylated hydroxytoluene (BHT) was used in both radical scavenging methods. Using the dose–response sigmoidal curve produced with OriginPro8 software (OriginLab, Northampton, Massachusetts, USA), the results for both procedures were reported as the concentration of samples giving 50% of radical scavenging activity (IC_{50}).

2.7. Antimicrobial activity of LSA-AgNPs and LSR-AgNPs

The antimicrobial activity of synthesized AgNPs by the aqueous leaf and root extracts of *L. salicaria* was tested on five Gram-negative and six Gram-positive bacterial strains. Antifungal effects of synthesized AgNPs were tested on the nine fungal species, eight molds and yeast *Candida albicans*. For the determination of AgNPs' antimicrobial activity, bacterial species were obtained from the Institute for Public Health in Kragujevac, Serbia, while fungal species were obtained from the Laboratory for Microbiology, Department of Biology and Ecology, Faculty of Science, University of Kragujevac, Serbia. Nutrient agar (NA) and Sabouraud Dextrose Agar (SDA) were used for the cultivation of bacterial strains and *C. albicans*, respectively, whereas potato glucose agar (PDA) was used for fungal strains growth before antimicrobial testing of AgNPs.

The antimicrobial activity of AgNPs was determined using the microdilution method for the determination of minimal inhibitory concentrations (MIC) described by Sarker *et al.*[18] The MIC determination assay was carried out by a serial dilution technique in 96-well microtiter plates using a Müller–Hinton broth (MHB) for bacterial and Sabouraud Dextrose Broth (SDB) for fungi and *C. albicans* testing. Fresh overnight cultures of bacteria and *C. albicans* were suspended in 5% DMSO and diluted with sterilized water to obtain a concentration of 1.0×10^6 CFU mL^{-1}.[19] The cell suspension of examined molds was diluted with 5% DMSO solution to obtain a concentration of 5×10^4 CFU mL^{-1} following NCCLS recommendations[20] for antifungal determination of AgNPs. For determination of MICs, AgNPs and antibiotic/antimycotic were dissolved in sterile water and 10 μL of these solutions were transferred to 96-microtiter wells containing 70 μL of MHB or SDB. The solution of resazurin (10 μL, 0.6 mg mL^{-1}), then, was added to 96-microtiter wells as an indicator of bacterial growth. In samples for antifungal determination, SBD was added instead of resazurin solution. Lastly, 10 μL of microorganisms' cell suspension was added to all the wells. The sterility control without suspension of microorganisms and growth control without antimicrobial compounds addition were also performed in each used 96-microtiter plate. The final concentration of tested AgNPs was in the range 0.156–20 mg mL^{-1}, while the concentrations of tested antibiotic (erythromycin) and antimycotic (nystatin) for MIC determination were in the range 0.3125–40 μg mL^{-1}. The lowest concentration of test sample in the well without color change of resazurin or visible growth was taken as the MIC value.

2.8. MTT cell proliferation assay

For determination of cytotoxicity of synthesized AgNPs, cancer cell lines Balb/c-3T3 mouse fibroblasts transformed by SV40 virus (SVT2 cells) and human epidermoid carcinoma cells (A431), as well as immortalized murine fibroblasts (Balb/c-3T3) and human keratinocytes (HaCaT) were used. Dulbecco's Modified Eagle's Medium with the addition of 2 mM L-glutamine, 10% fetal bovine serum, and streptomycin and penicillin was used for cell cultivation. Cells were cultured in an incubator containing 5% CO_2 at 37 °C. The cytotoxic activity of LSA-AgNPs and LSR-AgNPs was determined in 96-well plates with a cells density of 3×10^3 per well for immortalized cells and 2×10^3 per well for cancer cells. The solutions of LSA-AgNPs, in a concentration range from 1 to 25 μg mL^{-1} and LSR-AgNPs in a concentration range from 1 to 100 μg mL^{-1}, were added to 96-well plates, 24 h after plating the cells. The MTT (3-(4,5-dimethylthiazol-2-yl)-2,5-diphenyltetrazolium bromide) solution was added to each well (final MTT concentration MTT of 0.5 mg mL^{-1}) after 48 h of incubation.[21] Then plates were incubated at 37 °C for 4 h. After incubation, the solution of 2-propanol containing 0.01 N HCl was added to dissolve obtained formazan crystals. The absorbance at 570 nm of solution in each well was measured using an automatic plate reader (Microbeta Wallac 1420, PerkinElmer, Basel, Switzerland). The percentage of cell survival was calculated based on the percentage of viable cells in the presence of the tested AgNPs relative to untreated cells and cells supplied with equivalent quantities of the buffer. Each sample was tested in three independent assays.

2.9. Hemolytic activity of synthesized nanoparticles

The possible hemolytic activities of LSA-AgNPs and LSR-AgNPs were determined using erythrocyte cells and monitoring the level of released hemoglobin during incubation of tested samples with erythrocytes under simulated physiological conditions.[22] The human blood sample was collected from healthy volunteers in a sterile container with an anticoagulant (ethylenediaminetetraacetic acid). The blood sample was centrifugated at 2500 rpm for 10 min for isolation of erythrocytes. Obtained precipitates (red blood cells) were then washed three times using phosphate buffer saline (PBS, pH 7.4) and centrifuged. For determination of hemolytic properties, 1 mL of LSA-AgNPs or LSR-AgNPs solution in PBS was added in 1 mL of 5% red blood cells (RBCs) dissolved in PBS to obtain the final concentration of nanoparticles of 150, 120, 90, 60, 30, and 10 μg mL^{-1}. Negative control was prepared using PBS instead of nanoparticles solution, while the positive control contained 1 mL of RBCs and 1 mL 1% sodium dodecyl sulfate (SDS). The samples were incubated at 37 °C for 1 h and then centrifugated at 1200 rpm for 15 min. After centrifugation, the absorbance of the supernatant was measured spectrophotometrically at 540 nm. The following equation was used for the determination of the percentage of hemolyzed RBCs:

$$\%\ \text{Hemolysis} = \frac{\left(A_{\text{AgNPs}} - A_0\right) - A_k}{A_{\text{SDS}} - A_k} \times\ 100$$

where A_{AgNPs} is the absorbance of samples with AgNPs, A_0 is the absorbance of corresponding concentration of AgNPs in PBS, A_{SDS} is positive control with SDS solution, and A_k is negative control (only RBSs in PBS).

2.10. Catalytic degradation of Congo red and 4-nitrophenol

The evaluation of the catalytic activity of synthesized LSA-AgNPs and LSR-AgNPs was determined by the reduction of aqueous solutions of Congo red (CR) in the presence of $NaBH_4$ as described by Umamaheswari *et al.*[13] In this reaction, 1 mL of water solution of LSA-AgNPs or LSR-AgNPs (0.1 mg mL^{-1}) was mixed with 5 mL of 10 μM CR solution and 1.5 mL of 1 mM $NaBH_4$ solution. The rate of the catalytic degradation process of Congo red at different time intervals was monitored using a UV-Vis spectrophotometer (λ_{max} was at 497 nm).

The catalytic reduction of 4-nitrophenol (4-NP) using $NaBH_4$ in the presence of LSA-AgNPs and LSR-AgNPs was determined according to the method described by Desai *et al.*[23] Reaction solution was prepared by adding 0.5 mL of nanoparticles solution (0.3 mg mL^{-1}) to the mixture of 0.5 mL of $NaBH_4$ (0.05 mg mL^{-1}) and 5 mL of 4-NP (10 μg mL^{-1}) solutions. The reaction was monitored spectrophotometrically at 25 °C in the wavelength range from 250 to 550 nm.

The constant of reaction rate 'k' was calculated for catalytic degradation of CR and 4-NP using the following equation:

$$\ln\left(\frac{A_0}{A_t}\right) = kt$$

where 'A_0' is the absorbance at 0 min, 'A_t' is the absorbance at different times, 'k' is a constant of reaction, and 't' is reaction time.

3. Results and discussion

3.1. UV-Vis spectral analysis

The generation of AgNPs in solution during their synthesis using extracts was monitored spectrophotometrically. The color change of solutions from light yellow to dark brown and the appearance of the characteristic peak in UV-Vis spectra characteristic for AgNPs as a result of surface plasmon resonance (SPR) effect were observed. This process in a time-dependent manner was shown in Fig. 1A. The UV-Vis absorption spectra of formed nanoparticles were recorded (300–800 nm) and the highest peaks were positioned within 395–415 nm (characteristic peak for AgNPs), suggesting the formation of AgNPs. The maximum absorption values during biosynthesis were obtained at 30 min, and thereafter the absorption peaks did not increase, thus indicating the end of the synthesis process. Then, the influence of concentration of $AgNO_3$, extracts concentrations, temperature, and pH on the biosynthesis of nanoparticles using LSA and LSR aqueous extracts were evaluated. Initial conditions for the synthesis of both types of nanoparticles were 5 mM $AgNO_3$, 25 °C, 10% extracts concentration without adjustment of pH values. The separate UV spectra of the aerial part and root aqueous extracts are presented in Fig. 1S (ESI†). For the determination of the best conditions in the synthesis of AgNPs using

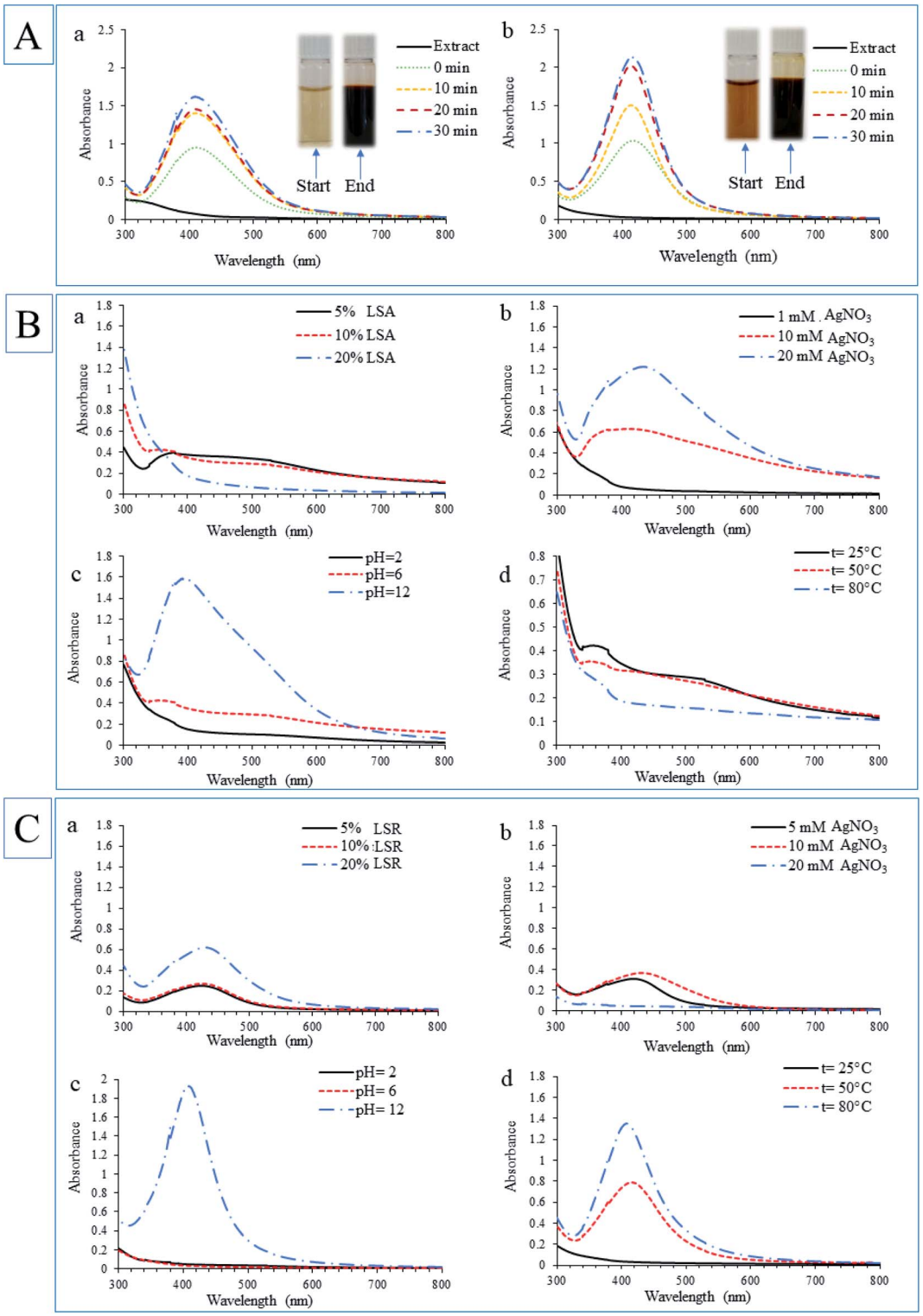

Fig. 1 (A) Time-dependent UV-Vis absorption spectra of AgNPs biosynthesized by *L. salicaria* aerial part (a) and root (b) extracts, (B) UV-Vis absorption spectra of LSA-AgNPs as a function of extract concentration (a), salt concentration (b), pH value of extract solution (c), and different temperatures (d), (C) UV-Vis absorption spectra of the LSR-AgNPs as a function of extract concentration (a), salt concentration (b), pH value of extract solution (c), and different temperatures (d).

LSA and LSR, the parameters were changed one by one. Fig. 1B shows the UV-Vis spectra for the LSA-AgNPs when applied different extract concentrations (a), salt concentrations (b), pH values (c), and temperatures (d). The concentration of 5% (v/v) of LSA extract was the most effective for AgNPs synthesis (Fig. 1B(a)), while higher concentrations of the extract caused agglomeration of nanoparticles and their precipitation. The sharpest peak of LSA-AgNPs was obtained using a higher salt

concentration (20 mM $AgNO_3$) (Fig. 1B(b)). Moreover, the application of 1 mM $AgNO_3$ did not lead to a high yield in nanoparticles synthesis. Increasing the pH value of LSA extract solution led to the augmentation of absorption values for LSA-AgNPs (Fig. 1B(c)). This can be explained by the assumption that the hydroxyl groups attract hydrogens of the phenolic and carboxyl groups (from flavonoids and phenolic acids) and thus increase the partial negative charge of oxygens which then more easily reduce the silver ions and stabilize formed nanoparticles.[24] It is also shown that the concentration of NaOH in solution during Ag^+ bioreduction has an effect on the size, shape, monodispersity, and yield of formed nanoparticles.[25] No nanoparticle formation was observed at pH 2, however, nanoparticles were successfully formed by increasing pH. The fast nanoparticle formation, with high intensity of SPR band at 394 nm, was observed at pH 12, indicating that alkaline conditions could be responsible for the activation of the compounds from the extract and make them more suitable electron donors. Also, Anigol *et al.* have shown that the synthesis of nanoparticles in an acidic medium produces a wide absorbance peak and a wide range of nanoparticles sizes. With the pH increase during synthesis, the peak was narrower and higher, while at pH 9 a more pronounced uniform nanoparticles size was observed.[26] Another study confirmed that pH change does not affect their shape while with increasing pH the size of nanoparticles decreases, for example, the average particle sizes of AgNPs on the pH 5, 7, and 9 range are 45, 29, and 20 nm, respectively.[27] The biosynthesis of LSA-AgNPs was also performed at different temperatures and based on the obtained absorption maximums, it can be concluded that temperature does not have an influence on the formation of nanoparticles using LSA. However, at lower temperatures, slightly higher peaks intensity in the UV-Vis absorption spectrum of LSA-AgNPs were noticed (Fig. 1B(d)). This may be an advantage of using LSA in the synthesis of nanoparticles compared with LSR, due to lower energy consumption during the synthesis process.

The spectrophotometric data for LSR-AgNPs synthesis under different conditions are shown in Fig. 1C. It was noticed that the absorption peaks for LSR-AgNPs increased dose-dependently with the increase of the extract concentration (Fig. 1C(a)). The sharpest peaks were obtained using 10 mM $AgNO_3$ for LSR-AgNPs synthesis. However, when a higher concentration of $AgNO_3$ (20 mM) was used for LSR-AgNPs synthesis, large, dispersed particles appeared, causing a lower absorption maximum in the UV-Vis spectrum (Fig. 1C(b)). As with the

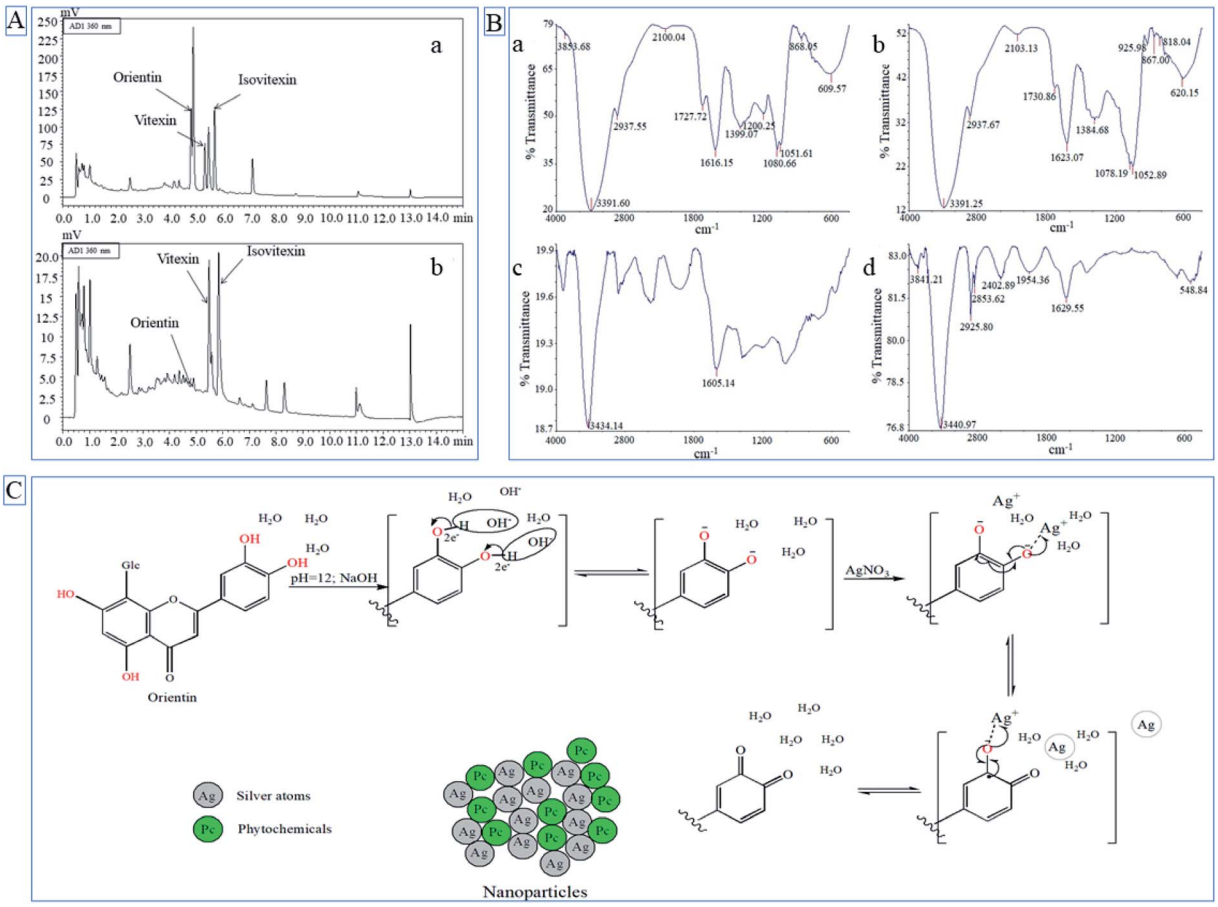

Fig. 2 (A) HPLC-PDA chromatograms of *L. salicaria* aerial part (a) and root (b) aqueous extracts, (B) FT-IR spectra of *L. salicaria* aerial part (a) and root extracts (b) and synthesized nanoparticles LSA-AgNPs (c) and LSR-AgNPs (d), (C) proposed mechanism of orientin Ag(I) reduction during nanoparticle synthesis.

Table 1 HPLC quantification of phenolic compounds and total phenolics (TP) and flavonoids (TF) content of *L. salicaria* aqueous extracts (LSA and LSR)[a]

	HPLC results (μg mL^{-1})			Spectrophotometric results	
Extracts	Orientin	Vitexin	Isovitexin	TP (mg GAE per g d.p.)	TF (mg QUE per g d.p.)
LSA	15.23 ± 0.06	6.94 ± 0.02	11.77 ± 0.17	99.56 ± 2.14	18.29 ± 0.95
LSR	0.357 ± 0.02	0.83 ± 0.02	1.46 ± 0.09	26.44 ± 0.81	0.19 ± 0.02

[a] d.p. – dry plant.

synthesis of nanoparticles using the aerial part extract, the influence of the pH value on LSR-AgNPs synthesis is clearly shown in Fig. 1C(c). Temperature change had a significant effect on the synthesis of LSR-AgNPs, in contrast to the synthesis of LSA-AgNPs. The UV-Vis absorption peak of the solution during LSR-AgNPs synthesis was much higher at 80 °C than at 50 and 25 °C, considering the same reaction conditions (Fig. 1C(d)).

Based on the presented results, the following conditions were used for further experiments. The synthesis of LSA-AgNPs was the most successful using the 5% aqueous extract, 20 mM $AgNO_3$ concentration, without heating, and pH 12, while the most favorable conditions for the synthesis of LSR-AgNPs are as follows, 20% aqueous extract, 10 mM $AgNO_3$, with heating at 80 °C for 30 min, and pH 12.

Our research is in accordance with studies conducted by Mohammadalinejhad *et al.* about the use of *L. salicaria* aerial part extract for the synthesis of AgNPs and AgNPs-organic nanohybrids.[16] The synthesis of nanoparticles using *L. salicaria* root extract, as well as the investigation of optimal conditions for the application of this plant in the synthesis of nanoparticles, their cytotoxic and photocatalytic activities, on the other hand, has never been reported before.

3.2. Phytochemical characterization of *L. salicaria* aqueous extracts

Aqueous extract of *L. salicaria* aerial part and root, used for the synthesis of AgNPs, contained total phenolic compounds in the concentration of 99.56 and 26.44 mg GAE per g of dry plant weight, respectively. Also, the aerial part of the plant had higher flavonoid content (18.29 mg QUE per g dry plant) than the root (0.19 mg QUE per g dry plant). These results, higher total phenolic and flavonoid content in aerial part, can explain the use of a lower concentration of LSA extract for AgNPs synthesis in comparison with the concentration of LSR extract. HPLC chromatograms of *L. salicaria* aerial part and root aqueous extracts are presented in Fig. 2A (a and b, respectively) while the quantification of identified phenolic compounds in extracts is given in Table 1. *C*-glucoflavones orientin, vitexin, and isovitexin were identified in both LSA and LSR aqueous extracts utilized for AgNPs synthesis. The presence of free hydroxyl groups in the structure of these compounds, which are responsible for the redox potential of polyphenolics, suggests that these *C*-glucoflavones may be one of the main compounds in extracts responsible to produce AgNPs. Plants with high antioxidant potential are strongly effective in converting metallic ions to metallic nanoparticles.[28] It is also well known that phenolic compounds are one of the most responsible metabolites for the antioxidant activity of plants, thus phenolics are considered as main contributors in the reduction of metal ions and the synthesis of nanoparticles using plant extracts.[29] HPLC analyses showed that LSA extract was richer in all identified compounds compared with LSR. In previous research published by Srećković *et al.* *C*-glucoflavones orientin and vitexin were also identified in *L. salicaria* methanol extracts as the main phenolic compounds.[15]

3.3. Characterization of synthesized AgNPs

3.3.1. XRPD analysis. The crystalline structure of the biosynthesized AgNPs was checked by XRPD analysis, and spectra of LSA-AgNPs and LSR-AgNPs are shown in Fig. 3A(a and b). Based on the obtained values of I/I_{max} intensities, mutual distances d, comparison with the literature data, and ICDD PDF-2 standards, the presence of the crystalline phases was confirmed.[30]

The most represented crystal phase in both samples was Ag (PDF 87-0597) and the next crystal phase by representation was an AgCl (PDF 31-1238). In the case of LSA-AgNPs (Fig. 5A), the characteristic Bragg reflection peaks appeared at position 38.19°, 44.42°, 64.53° and 77.46° in the 2θ range between 10° and 80°, which could be analog to the (111), (200), (220) and (311) planes of face-centered cubic (fcc) crystalline AgNPs.[1] The peaks at 27.80°, 32.24°, 46.24° correspond to the formation of AgCl phases. Silver in LSR-AgNPs had a lower crystallinity than silver chloride and lower crystallinity than silver in the LSA-AgNPs sample. However, the content of silver chloride in LSR-AgNPs was lower than in the LSA-AgNPs sample. The formation of the crystalline phase of silver chloride may be a consequence of the presence of chloride ions in plant extracts.

3.3.2. FTIR analysis. FT-IR spectra of the dried aqueous aerial part and root extracts of *L. salicaria* were compared with the spectrum of synthesized AgNPs (Fig. 2B). It was observed that the main peaks in the spectra of synthesized nanoparticles (Fig. 2B(c and d)) coincide with peaks of the corresponding extracts (Fig. 2B (a and b)). The absorption band at 3391.60 cm^{-1} for LSA and 3391.25 cm^{-1} for LSR extracts is the characteristic stretching vibration of –OH groups from phenolic compounds (flavonoids, phenolic acids, and other phenolic derivatives). The small band at 2937.55 cm^{-1} and 2937.67 cm^{-1} for LSA and LSR, respectively, may be a consequence of aliphatic

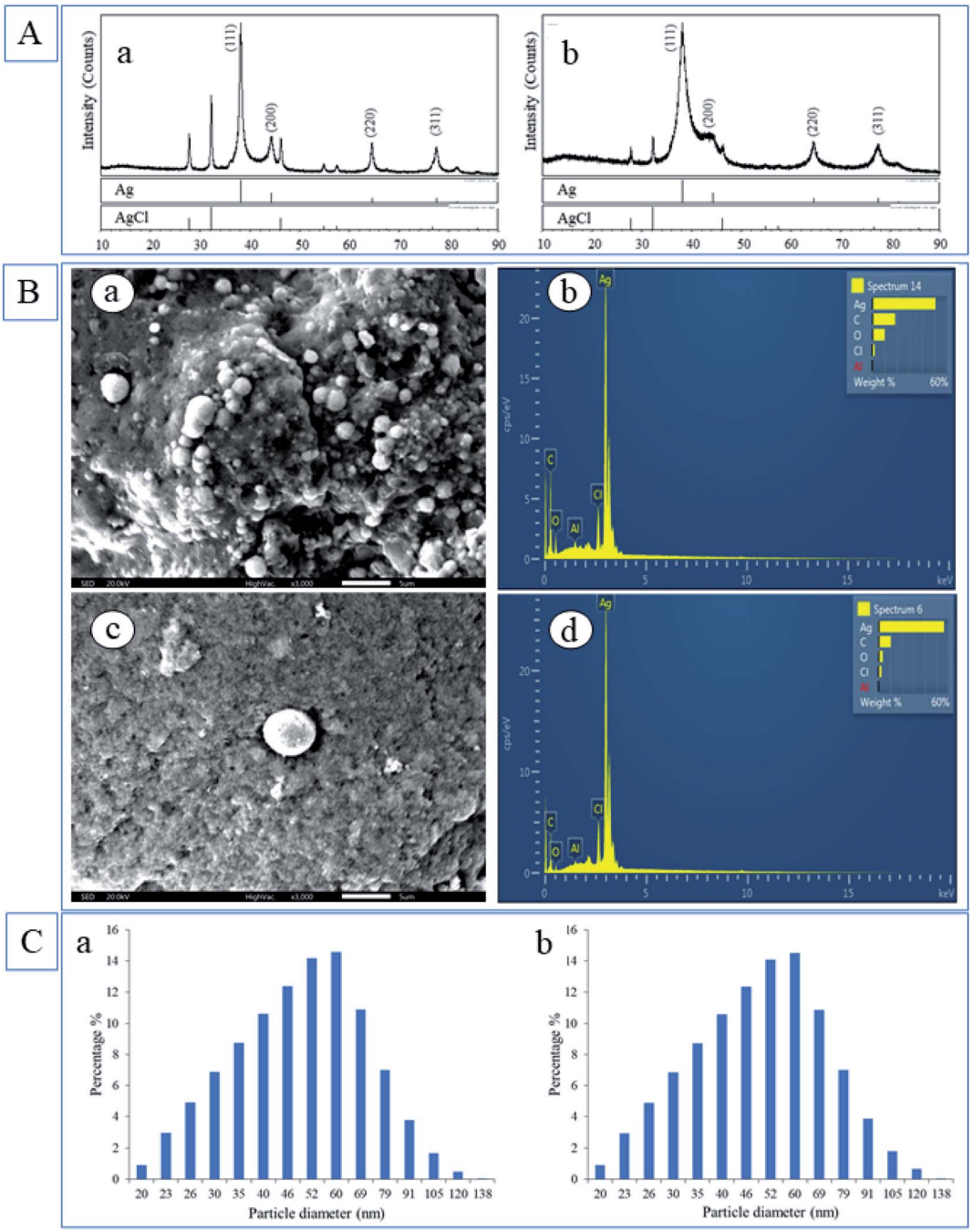

Fig. 3 (A) XRPD pattern of synthesized LSA-AgNPs (a) and LSR-AgNPs (b), (B) SEM image of biosynthesized LSA-AgNPs (a), LSR-AgNPs (c), and their corresponding EDX spectra (b and d), (C) particle size distributions of LSA-AgNPs (a) and LSR-AgNPs (b).

C–H stretching. Also, in the IR spectrum of the LSA and LSR extracts (Fig. 2B(a and b)), bands at 1727.72 and 1730.86 cm^{-1} indicate the presence of –C═O groups. The appearance of pronounced bands at 1616.15 cm^{-1} and 1623.07 cm^{-1} corresponds to the –C═C– of an aromatic ring. FTIR spectra of LSA-AgNPs (c) and LSR-AgNPs (d) were compared with the spectrum of LSA (a) and LSR (b). Based on Fig. 2B it is clear that LSA-AgNPs and LSR-AgNPs possessed bands that originated from plant extract. LSA-AgNPs and LSR-AgNPs possess bands at 3434.14 and 3440.97 cm^{-1}, respectively, which correspond to the alcohol groups, whereas LSR-AgNPs have bands at 2925.80 cm^{-1} that correspond to the C–H from alkanes. The appearance of these bands in LSA-AgNPs and LSR-AgNPs FTIR spectra implies that compounds from *L. salicaria* extracts be involved in the formation of nanoparticles' capping layer. However, peaks attributed to the –C═O group in the nanoparticles' spectra were reduced and almost merged with the intensive band corresponding to aromatic –C═C– vibrations (Fig. 2B(c and d)). The decrease in the peak intensity characteristic for the carbonyl group in nanoparticle spectra may be

attributed to the low concentration of compounds with this group were involving in the stabilization of nanoparticles. Also, the interaction of AgNPs with the carbonyl group (silver–carboxylate interactions) can decrease the intensity and position of –C═O peak in the FTIR spectrum.[31] Additionally, characteristic peaks at 1605.14 and 1629.55 cm^{-1} in obtained nanoparticles may correspond to –C═C– of an aromatic ring as confirmed in the extracts. Finally, the intense bands located at 1051.61–1052.89 cm^{-1} (Fig. 2B(a and b)) which correspond to the ether groups (C–O bond stretch) were present in LSA and LSR extracts (a and b) but not in LSR-AgNPs, so it can be assumed that compounds with an ether group are not responsible for the stabilization of root nanoparticles. The mentioned peaks in FTIR spectra of LSA-AgNPs and LSR-AgNPs characteristic for polyphenolic compounds indicate that flavonoids or other phenolic compounds form protective capping layers on the surface of the obtained nanoparticles. The disappearance of the bands at 1052.89, 1078.19, and 1384.68 cm^{-1} in LSR-AgNPs compared with LSR extract, proves that some compounds present in the extract do not participate in the stabilization of nanoparticles or may be chemically changed during bioreduction of metal ions.

3.3.3. SEM/EDX analysis. The results of SEM and EDX analyses for LSA-AgNPs and LSR-AgNPs are presented in Fig. 3B (a, b and c, d, respectively). The additional information about the structural morphology of green synthesized AgNPs was provided by SEM analysis, while EDX analysis was used to identify the elements included in LSA-AgNPs and LSR-AgNPs. Based on SEM results, it has been confirmed that the obtained nanoparticles possess a spherical shape, also a lower degree of agglomeration was observed. The observed large agglomerated nanoparticles probably occurred as a result of the evaporation of solvent during sample preparation.[32]

The EDX detection displayed intense signals of silver atoms in both types of nanoparticles, and it is around 3 KeV, which corresponds to the previously published value.[1] In addition to the Ag atoms as the main component of nanoparticles, the presence of C and O in LSA-AgNPs and LSR-AgNPs (Fig. 3B(b and d)) was also confirmed. The occurrence of C and O in nanoparticles may be the consequence of the presence of compounds from *L. salicaria* extracts incorporated into the nanoparticle structure. The elemental analysis of LSA-AgNPs and LSR-AgNPs by EDX (Fig. 3B (b and d)) showed that Ag is the main constituent, and it is found to be 50.92% and 45.66% respectively. The mineral content of the plant materials, which is mostly dependent on the soil of the plant habitat, results in the identification of Al traces in both types of nanoparticles. Vardanyan and Ingole confirmed the presence of Al in *L. salicaria*, which suggests the possibility of incorporation of these metal atoms into the structure of the obtained nanoparticles.[33] The Cl content may originate from plant extracts. Also, the increased content of C and O in the nanoparticles synthesized by the aerial part of the plant (LSA-AgNPs) corresponds to the higher phenolic content of the aerial part.

3.3.4. Particle dispersion characterization. For the determination of the size distribution profiles of LSA-AgNPs and LSR-AgNPs in solutions, DLS measurements were carried out. Besides the influence of the pH and temperature during the reaction of the synthesis, many biomolecules from the plant extracts (proteins, flavonoids, terpenoids, and other polyphenols) may have significant effects on the nanoparticle size, structure, and morphology.[8,34,35] Many studies have shown that the size of AgNPs is important for their stability, biocompatibility, and antibacterial activity.[36]

According to DLS analysis, LSA-AgNps and LSR-AgNPs possessed similar sizes, ranging from 20 to 138 nm (Fig. 3C). The size of the most formed LSA-AgNPs and LSR-AgNPs ranged between 35 and 60 nm (60.52 and 60.25% respectively), whereby 75.88% of particles were under 60 nm for both synthesized nanoparticles (Fig. 3C(a and b)). The complexity of the chemical composition of *L. salicaria* extracts may have significant effects on the agglomeration and deposition of the AgNPs.[14]

It is possible that the alkaline environment leads to an increase of negative charge of oxygen on the phenolic hydroxyl groups, which contributes to a better interaction between phytochemicals and silver ions, and therefore faster reduction time, and stabilization. Fig. 2C shows the possible mechanism of nanoparticles synthesis using orientin, one of the phenolic compounds (flavonoid) identified in both extracts used for nanoparticle synthesis. Bhutto *et al.* suggested a mechanism of AgNPs synthesis using gallic acid as an example of a phenolic compound, explaining that phenolic groups are oxidized to quinones.[37] Another study confirmed that flavonoids with 1 to 3 OH groups react only at pH values 9 and/or 10, while flavonoids with four and more hydroxyl groups, such as luteolin (aglycon of orientin), can reduce Ag^{+} relatively fast in the solution with pH around 7. The high reactivity of flavonoids in this process is conditioned by the presence of hydroxyl groups on the B ring which can be oxidized. Further, additional hydroxyl groups of flavonoids and their obtained oxidation forms after reduction reaction are important for attaching flavonoids molecules to obtained nanoparticles and for nanoparticles stabilization.[38] The orientin possesses these properties and may be one of the molecules in *L. salicaria* extracts that contributes to the formation and stabilization of AgNPs.

3.4. Antioxidant potential of *L. salicaria* aqueous extracts and synthesized nanoparticles

The antioxidant potential of the extracts was assessed using DPPH and ABTS methods. Butylated hydroxytoluene (BHT) was used as a referent standard and obtained results are presented in Table 2. The biosynthesized LSA-AgNPs and LSR-AgNPs displayed lower antioxidant activity in the DPPH method compared with LSA and LSR. It has been noticed that the IC_{50} value of the LSR-AgNPs in the ABTS assay was lower (127.78 μg mL^{-1}) compared with the IC_{50} value of LSA-AgNPs (141.66 μg mL^{-1}). Moreover, LSR-AgNPs showed higher antioxidant activity against $ABTS^{\bullet+}$ compared with the root aqueous extract (LSR).

As shown in Table 2 the aqueous extract of the aerial part had a slightly higher ABTS radical scavenging potential compared to the corresponding LSA-AgNPs nanoparticles. Interestingly, the nanoparticles synthesized by root extract (LSR-AgNPs) have approximately the two-fold ABTS radical scavenging potential

Table 2 *In vitro* antioxidant activity of *L. salicaria* aerial and root aqueous extracts and synthesized nanoparticles[a]

Samples and standards	IC_{50} values (μg mL^{-1})	
	DPPH$^{\bullet}$ scavenging activity	$ABTS^{\bullet+}$ scavenging activity
LSA	86.38 ± 0.13	65.33 ± 2.08
LSA-AgNPs	>100	141.66 ± 17.05
LSR	175.26 ± 6.31	198.36 ± 11.75
LSR-AgNPs	>100	127.78 ± 13.52
BHT	13.08 ± 0.97	21.29 ± 1.98

[a] LSA – *L. salicaria* aerial aqueous extract, LSR – *L. salicaria* root aqueous extract, LSA-AgNPs – silver nanoparticles synthesized by *L. salicaria* aerial part extract, LSR-AgNPs – silver nanoparticles synthesized by *L. salicaria* root extract.

Table 3 Antibacterial and antifungal activity of AgNPs synthesized by *L. salicaria* aerial part (LSA-AgNPs) and root (LSR-AgNPs) extracts

Bacterial strains	MIC (mg mL^{-1})		MIC (μg mL^{-1})
	LSA-AgNPs	LSR-AgNPs	Erythromycin
E. coli	0.625	2.5	2.5
B. cereus	0.3125	0.3125	<0.156
P. aeruginosa	<0.156	0.3125	20
E. faecalis	0.3125	0.625	1.25
B. subtilis	0.156	0.625	10
M. lysodeikticus	0.625	0.156	<0.156
S. typhimurium	1.25	0.625	2.5
S. enteritidis	1.25	0.625	20
S. epidermidis	<0.156	0.3125	0.625
S. aureus	0.3125	0.625	1.25
K. pneumoniae	0.3125	0.625	10
Fungal strains	**MIC (mg mL^{-1})**		**MIC (μg mL^{-1})**
	LSA-AgNPs	LSR-AgNPs	Nystatin
C. albicans	0.625	1.25	1.25
T. longibrachiatum	1.25	1.25	5
T. harzianum	1.25	0.625	5
P. canescens	0.3125	0.625	2.5
P. cyclopium	<0.156	0.625	2.5
D. stemonitis	2.5	0.625	2.5
A. alternata	1.25	0.3125	1.25
F. oxysporum	10	0.625	2.5
A. brasiliensis	10	0.3125	1.25

compared to the aqueous root extract. Previous studies have confirmed that nanoparticles synthesized using plant extracts possessed significantly higher antioxidant potential than nanoparticles obtained using conventional methods indicating that plant compounds bound to nanoparticles are responsible for the higher antioxidant potential.[39] The higher antioxidant potential of LSR-AgNPs, compared with the value obtained with LSR, may suggest that this extract has antioxidant compounds that can be incorporated very efficiently on the surface of the nanoparticles.

3.5. Antimicrobial activity

The employment of silver as an antimicrobial agent against infections has been known since ancient Greek and Roman times. Numerous studies have confirmed the antimicrobial properties of AgNPs on different microbes, fungi, and parasites.[2,40] According to our knowledge, most studies dealing with the antimicrobial activity of AgNPs used the disk diffusion test to determine the antimicrobial activity of nanoparticles samples. The disk diffusion test is used to determine the antimicrobial susceptibility of microorganisms against antimicrobial drugs, while the dilution method provides significantly more accurate results, and obtained MIC values are used for the determination of drug dosage for infection treatment.[41] In this study, the microdilution method was used for the determination of the antimicrobial activity of synthesized LSA-AgNPs and LSR-AgNPs and the results are presented in Table 3. The obtained nanoparticles showed potent antibacterial activity with MIC values below 1 mg mL^{-1} against the tested bacteria. Antibacterial activities of LSR-AgNPs and LSA-AgNPs were similar and most of their MIC values were in the range from 0.156 to 0.625 mg mL^{-1}. Obtained nanoparticles showed less antifungal activity compared with their antibacterial potential, especially LSA-AgNPs. The concentrations that inhibit fungal growth were considerably lower for tested LSR-AgNPs compared with LSA-AgNPs which showed MIC values for six fungal species above 1 mg mL^{-1}.

It may be interesting to point out that AgNPs synthesized using LSA and LSR extracts showed higher inhibitory potential on the growth of *P. aeruginosa* compared to AgNPs synthesized using *P. hibiscicola* in research conducted by Punjabi *et al*[42] Another Lythraceae plant, *Lagerstroemia speciosa*, was used to synthesis Ag-NPs that inhibited biofilm formation against *P. aeruginosa*.[43] There are few studies reporting the MIC values of AgNPs determined using the dilution method technique, a number of studies are based on the disk diffusion method for the determination of the antimicrobial activity of AgNPs. Garibo *et al.* showed that green synthesized AgNPs possess higher antimicrobial potential against *E. coli*, *S. aureus*, *P. aeruginosa*, and *C. albicans* than chemically produced AgNPs.[44] Also, the study conducted by Shu *et al.* confirmed that ampicillin in combination with AgNPs possesses extremely higher antibacterial activity against highly resistant *E. coli*-Amp^{+} compared with ampicillin alone.[7] Using electron microscopy, Xia *et al.* demonstrated that AgNPs destroy the cell wall, infiltrate within the cells, damage organelles, induce chromatin condensation and margination, a sign of apoptotic cell death.[45] Also, it has been confirmed that the size of nanoparticles has an influence on their antimicrobial activity, smaller-sized nanoparticles pass unhindered through the cell membrane, expressing their activity within the cell. According to reported studies, the antimicrobial activity of AgNPs is also attributed to the electrostatic interaction between positively charged silver ions and negatively charged cell walls.[46] Due to a slightly different cell membrane of the fungi composed mostly of fibrous β-1,3 glucan

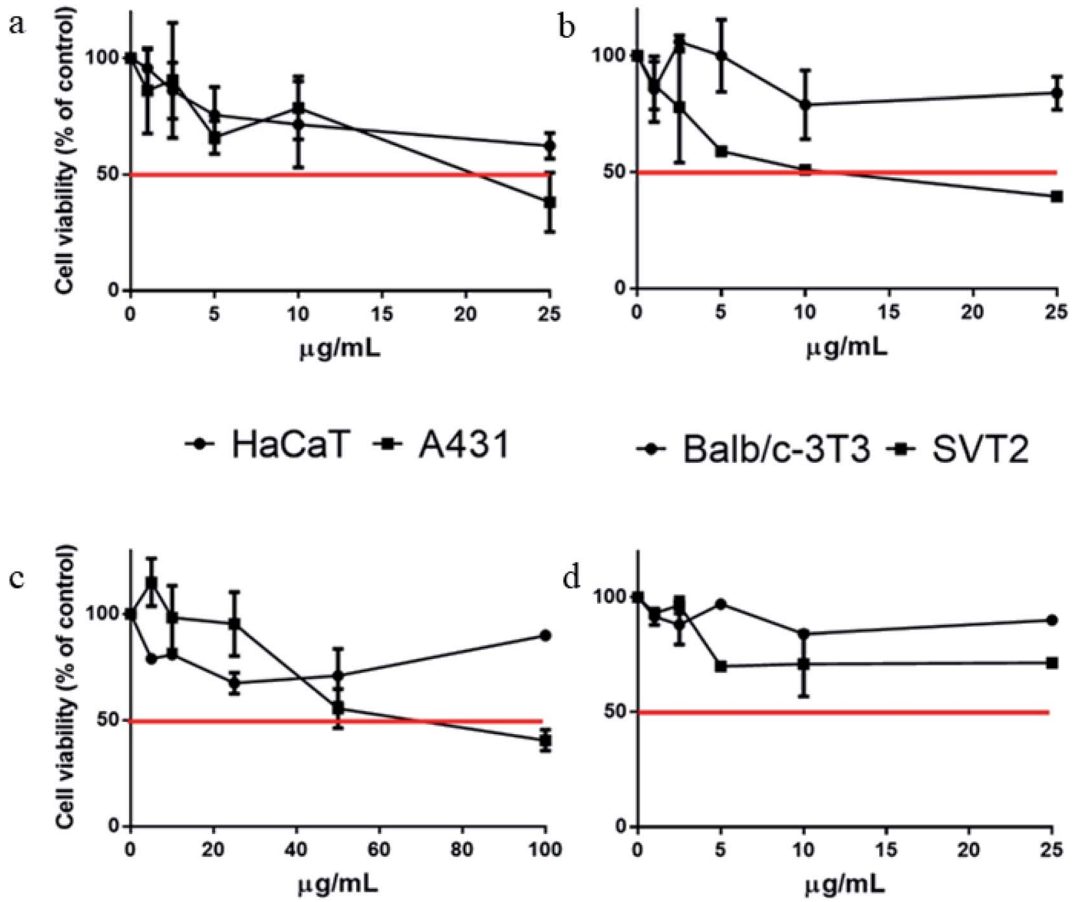

Fig. 4 Cytotoxic activity of synthesized LSA-AgNPs (a and b) and LSR-AgNPs (c and d) against immortalized (HaCaT and Balb/c-3T3) and cancer (A431 and SVT-2) cell lines.

and mannoproteins, interaction with AgNPs is quite different.[47] This fact may be one of the causes for the slightly lower antifungal activity of obtained AgNPs compared with their antibacterial activity.

3.6. Cytotoxic activity

The cytotoxic activity of biosynthesized LSA-AgNPs and LSR-AgNPs was analyzed on two immortalized (murine fibroblasts Balb/c-3T3, and human keratinocytes, HaCaT) cell lines and two cancer cell lines (transformed fibroblast, SVT2, and epidermoid carcinoma, A431). The MTT test was used to determine cell viability after the treatment with different concentrations of LSA-AgNPs and LSR-AgNPs (from 1 to 100 g mL^{-1}) for 48 hours.

As shown in Fig. 4 (panels a and b), LSA-AgNPs present a slight selectivity towards cancer A431 and SVT-2 cells, with IC_{50} values of 20.5 ± 5 and 12,7 ± 6 μg mL^{-1}, respectively. Interestingly, no IC_{50} values were detected on immortalized cells. In a previously published research, the methanolic extract of the *L. salicaria* root showed biocompatibility on the two immortalized cell lines, but only up to 45 μg mL^{-1} for murine cell lines.[15] Interestingly, when roots were used to obtain nanoparticles, LSR-AgNPs exerted toxicity only towards the A431 cell line (62 ± 17 μg mL^{-1}) (panels c and d). Based on the presented results, both nanoparticles LSA-AgNPs and LSR-AgNPs synthesized using *L. salicaria* aqueous extracts, exhibit a selective behavior towards cancer cell lines. Thus, the selective activity may occur due to the acidic pH in cancer cells, leading to greater release of Ag^{+} and phytochemicals from AgNPs in their surroundings compared with the immortalized ones.[48] The cytotoxicity of AgNPs is based on their ability to penetrate into the cells and liberate silver ions which promote ROS generation, causing mitochondrial and DNA damage, as well as cell apoptosis.[49] In addition, the advantage of AgNPs synthesized by plant extracts is based on phytochemicals incorporated

Table 4 Percentage of hemolysis induced by AgNPs synthesized by aerial part (LSA-AgNPs) and root (LSR-AgNPs) extracts

Concentration (μg mL^{-1})	% hemolysis	
	LSA-AgNPs	LSR-AgNPs
150	<negative control	2.77 ± 0.25
120	<negative control	0.50 ± 0.11
90	<negative control	0.28 ± 0.06
60	<negative control	<negative control
30	<negative control	<negative control
10	<negative control	<negative control

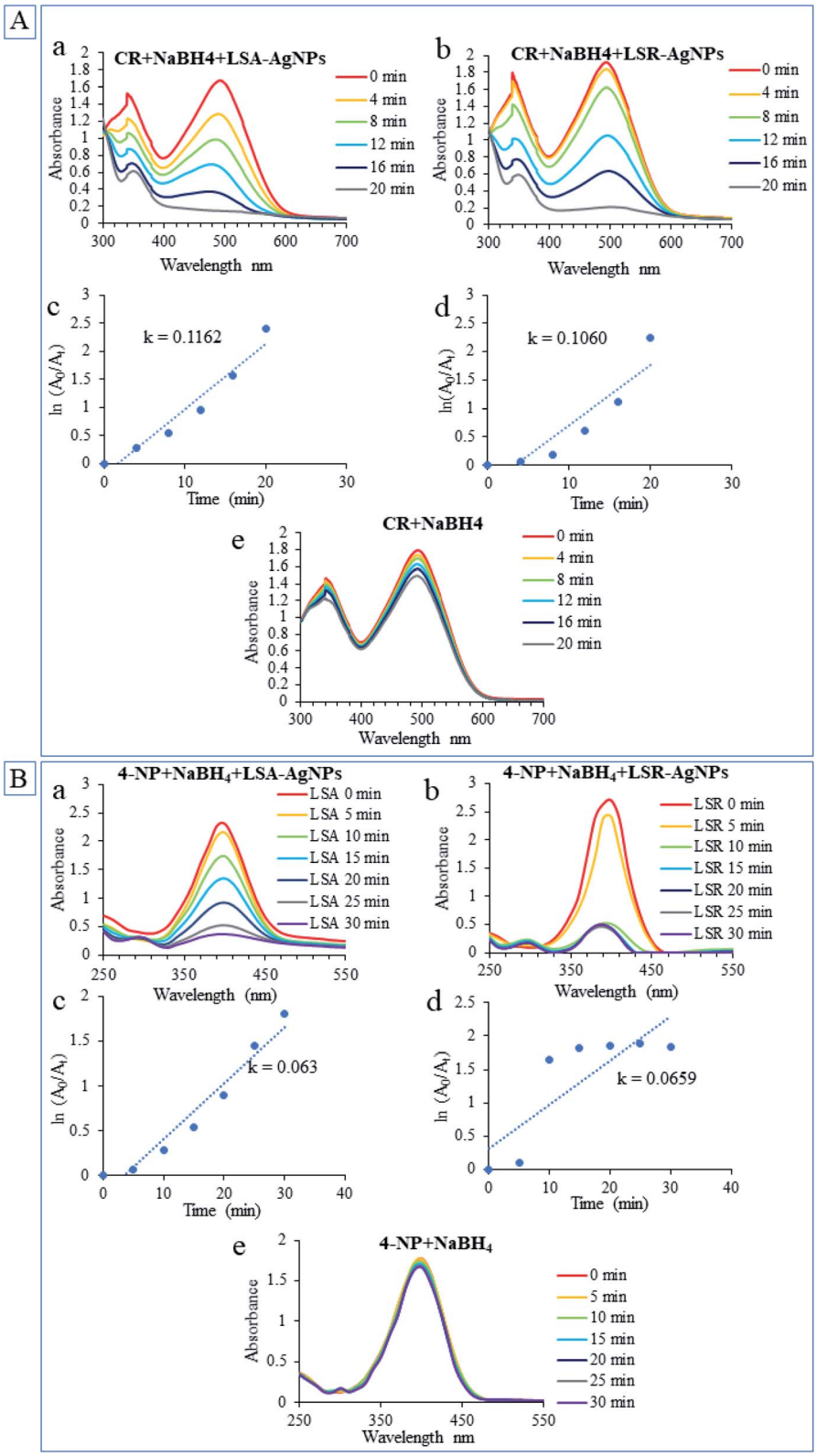

Fig. 5 (A) The catalytic activity of the synthesized LSA-AgNPs (a) and LSR-AgNPs (b) on Congo red (CR) degradation in the presence of $NaBH_4$ and corresponding degradation kinetics of CR (c and d), degradation of CR in absence of nanoparticles (e); (B) the catalytic activity of the synthesized LSA-AgNPs (a) and LSR-AgNPs (b) on reduction 4-NP to 4-AP in the presence of $NaBH_4$ and corresponding degradation kinetics of 4-NP (c and d), degradation of 4-NP in absence of nanoparticles (e).

into the nanoparticle structure, which have well-known biological activity. Various studies concluded that green synthesized AgNPs combined with cancer drugs can elevate anticancer activity, in relation to the drugs attached to chemically synthesized nanoparticles.[50]

3.7. Hemolytic activity of synthesized nanoparticles

Blood is the first contact for nanoparticles to reach their target tissues, so the effect of nanoparticles on blood cells is crucial for further research and potential therapeutic application.[51] The process of hemoglobin release during the interaction of different LSA-AgNPs and LSR-AgNPs concentrations with erythrocytes at 37 °C for 1 h was monitored spectrophotometrically at 540 nm. The hemolytic activity of the sample was calculated based on the hemolytic activity of SDS used as a positive control. It is considered that 1% solution of SDS causes complete (100%) hemolysis of erythrocytes. The examined samples of nanoparticles showed a negligible degree of erythrocytes hemolysis (Table 4). Moreover, LSA-AgNPs at all applied concentrations showed lower hemolytic activity compared with the negative control (erythrocytes in PBS solution), hence LSA-AgNPs may be considered as membrane stabilizing agents. However, LSR-AgNPs showed dose-dependent weak hemolysis when applied in concentrations from 150 to 90 μg mL^{-1}. The highest applied concentration of LSR-AgNPs showed only 2.8% of erythrocytes hemolysis while concentrations lower than 90 μg mL^{-1} had no effect on erythrocyte degradation. Because high hemocompatibility of biosynthesized nanoparticles was observed, it could be safely used in a therapeutic application, moreover, LSA-AgNPs possess the potential for further research as antihemolytic and erythrocytes membrane stabilization agents.

3.8. The catalytic activity of synthesized nanoparticles

Environmental pollution by industrial dyes has a great influence on public health. Many of the synthetic dyes are highly carcinogenic and left in the environment for a long time. As degradation of these compounds requires catalysts that would increase the reaction rate, today, there is great interest in the easy production of environmentally friendly catalysts.[52] Many investigations have confirmed that green synthesis nanoparticles had the potential to catalyze the degradation of numerous organic contaminants. The effectiveness of LSA-AgNPs and LSR-AgNPs for the degradation of CR and the reduction of 4-nitrophenol to 4-aminophenol (4-AP) at room temperature was examined. The reactions of catalytic degradation of CR were monitored spectrophotometrically in the wavelength range between 700 and 300 nm, while the wavelength range for monitoring 4-NP reduction was between 550 and 250 nm. The ability of AgNPs to behave as a catalyst in the degradation of dye is reflected in their property to transfer an electron from donor molecules ($NaBH_4$) to acceptor molecules (azo bond in CR).[53] The catalytic activities of LSA-AgNPs and LSR-AgNPs are presented in Fig. 5 and both types of nanoparticles showed high potential for catalytic degradation of CR (Fig. 5A(a and b)) as well as for catalytic reduction 4-NP to 4-AP in the presence of $NaBH_4$ (Fig. 5B(a and b)). The absorbance of the CR constantly decreased overtime at 338 and 497 nm, and finally, the solution became colorless and absorption maximums in the UV-Vis spectrum disappear. Application of $NaBH_4$ in the absence of AgNPs has no significant effect on the degradation of CR solution and reduction 4-NP (Fig. 5A and B(e)). During the reduction process of CR and 4-NP, $NaBH_4$ has the role of an electron source, however, electron transfer is not possible without the presence of a catalyst. The nanoparticles serve as electron transporters, absorbing BH_4^- and dyes on their surface, allowing electron exchange from BH_4^- to organic dyes.[54] The catalytic rate constant (k) for LSA-AgNPs and LSR-AgNPs was higher for reaction of degradation CR ($k = 0.1162$ and $k = 0.1060$, respectively) compared with k for chemocatalytic reduction of 4-NP to 4-AP ($k = 0.063$ and $k = 0.0659$, respectively). In general, biogenic LSA-AgNPs and LSR-AgNPs exhibited excellent catalytic activity with high efficiency of CR degradation and 4-NP reduction, so they can be successfully applied as catalysts in wastewater treatment.

4. Conclusions

The results of the present study showed that aqueous extracts of *Lythrum salicaria* can be successfully used for the eco-friendly, economically viable, and rapid synthesis of AgNPs. It is concluded that reaction conditions play an important role in the rate of nanoparticles formation. The results of antimicrobial activity demonstrate that newly synthesized AgNPs have promising antimicrobial potential against most of the selected bacteria. Their activity on immortalized and cancer cells indicates a selectivity towards the latter, even if low toxicity was found in the case of LSR-AgNPs towards SVT-2 cells. Contrary LSR-AgNPs which showed a slight degree of red blood cell hemolysis at the highest applied concentration, LSA-AgNPs are completely hemocompatible. The green AgNPs showed clear catalytic potential in Congo red dye and 4-nitrophenol degradation reactions, which possesses well-known harmful effects on the environment. The current study suggested that the invasive potential of this plant in the North American continent may be exploited in the eco-fabrication of AgNPs. Further research will be focused on decreasing size and increasing the cytotoxic selectivity of synthesized nanoparticles. Also, further research may include the incorporation of some drugs into their structure for the development of new pharmaceuticals. Due to the demonstrated antimicrobial activity, future research may be focused on the possible use of biosynthesized nanoparticles in wastewater disinfection as well.

Conflicts of interest

There are no conflicts to declare.

Acknowledgements

This work was supported by the Serbian Ministry of Education, Science and Technological Development (Agreements No. 451-03-9/2021-14/200122 and No. 451-03-9/2021-14/200378).

References

1 A. A. Abdelhamid, M. A. Al-Ghobashy, M. Fawzy, M. B. Mohamed and M. M. S. A. Abdel-Mottaleb, *ACS Sustainable Chem. Eng.*, 2013, **1**, 1520–1529.
2 P. Singh, Y. J. Kim, D. Zhang and D. C. Yang, *Trends Biotechnol.*, 2016, **34**, 588–599.
3 M. Guilger-Casagrande and R. de Lima, *Front. Bioeng. Biotechnol.*, 2019, **7**, 287.
4 Z. Yang, Z. Li, X. Lu, F. He, X. Zhu, Y. Ma, R. He, F. Gao, W. Ni and Y. Yi, *Nano-Micro Lett.*, 2016, **9**, 1–13.
5 M. S. Akhtar, J. Panwar and Y. S. Yun, *ACS Sustainable Chem. Eng.*, 2013, **1**, 591–602.
6 N. Kulkarni and U. Muddapur, *J. Nanotechnol.*, 2014, **2014**, 510246.
7 M. Shu, F. He, Z. Li, X. Zhu, Y. Ma, Z. Zhou, Z. Yang, F. Gao and M. Zeng, *Nanoscale Res. Lett.*, 2020, **15**, 1–9.
8 H. P. Borase, B. K. Salunke, R. B. Salunkhe, C. D. Patil, J. E. Hallsworth, B. S. Kim and S. V. Patil, *Appl. Biochem. Biotechnol.*, 2014, **173**, 1–29.
9 R. Dobrucka, M. Szymanski and R. Przekop, *Int. J. Environ. Sci. Technol.*, 2019, **16**, 8517–8526.
10 A. M. Youssef, H. S. El-Sayed, I. EL-Nagar and S. M. El-Sayed, *RSC Adv.*, 2021, **11**, 22571–22584.
11 D. Rawat, V. Mishra and R. S. Sharma, *Chemosphere*, 2016, **155**, 591–605.
12 N. Kataria and V. K. Garg, *J. Environ. Chem. Eng.*, 2017, **5**, 5420–5428.
13 C. Umamaheswari, A. Lakshmanan and N. S. Nagarajan, *J. Photochem. Photobiol., B*, 2018, **178**, 33–39.
14 J. P. Piwowarski, S. Granica and A. K. Kiss, *J. Ethnopharmacol.*, 2015, **170**, 226–250.
15 N. Srećković, J. S. Katanić Stanković, S. Matić, N. R. Mihailović, P. Imbimbo, D. M. Monti and V. Mihailović, *Ind. Crops Prod.*, 2020, **155**, 112781.
16 S. Mohammadalinejhad, H. Almasi and M. Esmaiili, *Mater. Sci. Eng., C*, 2019, **105**, 110115.
17 V. Mihailović, S. Kreft, E. T. Benković, N. Ivanović and M. S. Stanković, *Ind. Crops Prod.*, 2016, **89**, 141–151.
18 S. D. Sarker, L. Nahar and Y. Kumarasamy, *Methods*, 2007, **42**, 321–324.
19 CLSI, *Reference Method for Broth Dilution Antifungal Susceptibility Testing of Yeasts, Approved Standard — Second Edition Serving the World ' s Medical Science Community Through Voluntary Consensus*, 2008, vol. 22.
20 NCCLS, *Reference Method for Broth Dilution Antifungal Susceptibility Testing of Yeasts; Approved Standard — Second Edition. NCCLS document M27-A2*, NCCLS, 940 West Valley Road, Suite 1400, Wayne, Pennsylvania 19087-1898 USA, 2nd edn, 2002, vol. 22.
21 M. E. Cucciolito, A. D'Amora, G. De Feo, G. Ferraro, A. Giorgio, G. Petruk, D. M. Monti, A. Merlino and F. Ruffo, *Inorg. Chem.*, 2018, **57**, 3133–3143.
22 A. Ullah Khan, Q. Ullah Khan, K. Tahir, S. Ullah, A. Arooj, B. Li, K. Ur Rehman, S. Nazir, M. Ullah Khan and I. Ullah, *Mater. Sci. Eng., C*, 2021, **126**, 112146.
23 M. P. Desai, R. V. Patil and K. D. Pawar, *Process Biochem.*, 2020, **98**, 172–182.
24 A. M. El Badawy, T. P. Luxton, R. G. Silva, K. G. Scheckel, M. T. Suidan and T. M. Tolaymat, *Environ. Sci. Technol.*, 2010, **44**, 1260–1266.
25 G. Liu, X. Ma, X. Sun, Y. Jia and T. Wang, *Adv. Mater. Sci. Eng.*, 2018, 3758161.
26 L. B. Anigol, J. S. Charantimath and P. M. Gurubasavaraj, *Org. Med. Chem. Int. J.*, 2017, **3**(5), 555622.
27 T. N. Jebakumar Immanuel Edison and M. G. Sethuraman, *ACS Sustainable Chem. Eng.*, 2013, **1**, 1326–1332.
28 V. Goodarzi, H. Zamani, L. Bajuli and A. Moradshahi, *Mol. Cell Biol. Res. Commun.*, 2014, **3**, 165–174.
29 S. Firoozi, M. Jamzad and M. Yari, *J. Nanostruct. Chem.*, 2016, **6**, 357–364.
30 S. Pirtarighat, M. Ghannadnia and S. Baghshahi, *Mater. Sci. Eng., C*, 2019, **98**, 250–255.
31 V. Thi Lan Huong and N. T. Nguyen, *Mater. Today: Proc.*, 2019, **42**, 88–93.
32 V. Seerangaraj, S. Sathiyavimal, S. N. Sankar, J. G. T. Nandagopal, P. Balashanmugam, F. A. Al-Misned, M. Shanmugavel, P. Senthilkumar and A. Pugazhendhi, *J. Environ. Chem. Eng.*, 2021, 105088.
33 L. G. Vardanyan and B. S. Ingole, in *Environment International*, Elsevier Ltd, 2006, vol. 32, pp. 208–218.
34 E. Navarro, A. Baun, R. Behra, N. B. Hartmann, J. Filser, A. J. Miao, A. Quigg, P. H. Santschi and L. Sigg, *Ecotoxicology*, 2008, **17**, 372–386.
35 K. L. Kelly, E. Coronado, L. L. Zhao and G. C. Schatz, *J. Phys. Chem. B*, 2003, **107**, 668–677.
36 M. José Yacamán, J. A. Ascencio, H. B. Liu and J. Gardea-Torresdey, *J. Vac. Sci. Technol., B: Microelectron. Nanometer Struct. Process., Meas., Phenom.*, 2001, **19**, 1091–1103.
37 A. A. Bhutto, Ş. Kalay, S. T. H. Sherazi and M. Culha, *Talanta*, 2018, **189**, 174–181.
38 M. Švecová, P. Ulbrich, M. Dendisová and P. Matějka, *Spectrochim. Acta, Part A*, 2018, **195**, 236–245.
39 F. U. Khan, Y. Chen, N. U. Khan, Z. U. H. Khan, A. U. Khan, A. Ahmad, K. Tahir, L. Wang, M. R. Khan and P. Wan, *J. Photochem. Photobiol., B*, 2016, **164**, 344–351.
40 C. Vijilvani, M. R. Bindhu, F. C. Frincy, M. S. AlSalhi, S. Sabitha, K. Saravanakumar, S. Devanesan, M. Umadevi, M. J. Aljaafreh and M. Atif, *J. Photochem. Photobiol., B*, 2020, **202**, 111713.
41 H. Liu, T. H. Taylor, K. Pettus, S. Johnson, J. R. Papp and D. Trees, *Antimicrob. Resist. Infect. Control*, 2016, **5**, 1–6.
42 K. Punjabi, S. Mehta, R. Chavan, V. Chitalia, D. Deogharkar and S. Deshpande, *Front. Microbiol.*, 2018, **9**, 2207.
43 V. Sai Saraswathi, N. Kamarudheen, K. V. BhaskaraRao and K. Santhakumar, *J. Photochem. Photobiol., B*, 2017, **168**, 107–116.
44 D. Garibo, H. A. Borbón-Nuñez, J. N. D. de León, E. García Mendoza, I. Estrada, Y. Toledano-Magaña, H. Tiznado, M. Ovalle-Marroquin, A. G. Soto-Ramos, A. Blanco, J. A. Rodríguez, O. A. Romo, L. A. Chávez-Almazán and A. Susarrey-Arce, *Sci. Rep.*, 2020, (10), 1–11.

45 Z. K. Xia, Q. H. Ma, S. Y. Li, D. Q. Zhang, L. Cong, Y. L. Tian and R. Y. Yang, *J. Microbiol., Immunol. Infect.*, 2016, **49**, 182–188.
46 J. S. Kim, E. Kuk, K. N. Yu, J. H. Kim, S. J. Park, H. J. Lee, S. H. Kim, Y. K. Park, Y. H. Park, C. Y. Hwang, Y. K. Kim, Y. S. Lee, D. H. Jeong and M. H. Cho, *Nanomedicine*, 2007, **3**, 95–101.
47 K. J. Kim, W. S. Sung, B. K. Suh, S. K. Moon, J. S. Choi, J. G. Kim and D. G. Lee, *BioMetals*, 2009, **22**, 235–242.
48 I. F. Tannock and D. Hot, *Acid pH in Tumors and Its Potential for Therapeutic Exploitation1*, 1989.
49 T. Shi, X. Sun and Q.-Y. He, *Curr. Protein Pept. Sci.*, 2018, **19**, 525–536.
50 S. Patra, S. Mukherjee, A. K. Barui, A. Ganguly, B. Sreedhar and C. R. Patra, *Mater. Sci. Eng., C*, 2015, **53**, 298–309.
51 K. M. de la Harpe, P. P. D. Kondiah, Y. E. Choonara, T. Marimuthu, L. C. du Toit and V. Pillay, *Cells*, 2019, **8**(10), 1209.
52 A. Naghizadeh, Z. M. Mizwari, S. M. Ghoreishi, S. Lashgari, S. Mortazavi-Derazkola and B. Rezaie, *Environ. Technol. Innovation*, 2021, **23**, 101560.
53 H. Kolya, P. Maiti, A. Pandey and T. Tripathy, *J. Anal. Sci. Technol.*, 2015, **6**, 1–7.
54 K. Zhang, J. M. Suh, J.-W. Choi, H. W. Jang, M. Shokouhimehr and R. S. Varma, *ACS Omega*, 2019, **4**, 483–495.